Transition Metal Chemistry (2023) 48:307–314
https://doi.org/10.1007/s11243-023-00544-9

Design and fabrication of novel coordination polymers containing Co(II), Ni(II), and Cu(II) for electrochemical detection of both ascorbic acid and Cr(VI)

Xiaohui Li[1] · Bingqian Wang[2] · Yue Gao[1] · Guocheng Liu[1,2] · Xiuli Wang[1]

Received: 8 April 2023 / Accepted: 9 July 2023 / Published online: 9 August 2023

Abstract

For the rapid detection of ascorbic acid (AA) and Cr(VI), three novel 2D coordination polymers (CP) with different metal centers [Co(L)(5-NIPA)(H_2O)]·H_2O (**1**), [Ni(L)(5-NIPA)(H_2O)]·H_2O (**2**) and [Cu(L)(5-NIPA)]·H_2O (**3**) were synthesized by the traditionally hydrothermal method (L = N,N′-bis(pyridine-3-ylmethyl)-4-(4-carboxybenzyl)oxybenzamide, 5-NIPA = 5-nitroisophthalic acid). CPs **1** and **2** are isomorphic 2D regular (4,4)-connected networks, and CP **3** has a twisted 2D lamellar structure. All of the above complexes present highly sensitive and selective electrocatalytic sensing performances for AA and Cr(VI). The detection limits of the three complexes were 0.320, 3.360 and 3.600 μM for AA, and 0.2349, 0.9928 and 3.6054 μM for Cr(VI), respectively.

Introduction

With the rapid development of society and technology, while enjoying convenient life, people's health is also under various threats from diet or the environment. For instance, ascorbic acid (AA) commonly known as vitamin C is an essential nutrient to increase the immunity and prevent the harm of free radicals to human body [1]. However, excessive intake of AA may also cause lithiasis and gastrointestinal diseases [2, 3]. Apart from dietary issues, environmental pollution also has a great impact on human health. For example, $Cr_2O_7^{2-}$ and CrO_4^{2-} as powerful oxidants have been widely used in chemical industry, resulting in a large amount of wastewater containing Cr. Among various valence states of Cr, Cr(VI) are the most toxic, which may lead to many serious diseases such as dermatitis, chronic ulcers and cancers [4, 5]. Therefore, it is crucial to find a convenient, rapid and efficient method for the detection of AA in body fluids and Cr(VI) in industrial wastewater. Different methods have been applied to detect AA and Cr(VI), such as spectrophotometric [6], fluorescence [7], liquid chromatography [8] and electrochemical method [9, 10]. It has been reported that a fluorescent probe with rhodamine B embedded in zinc metal–organic framework (Zn-MOF) has been invented for the detection of AA [11]. A mixed valence state Ce-MOF sensor was used for fluorescence detection of AA [12]. MOFs based on Cu^{2+} and Eu^{3+} ions were used for photoluminescence detection of AA [10]. A new U-shaped bending fiber optic sensor (U-FOS) probe was applied to detect Cr(VI) [13]. Novel thorium-based MOFs constructed with thorium cations and tetraphenylvinyl ligands for fluorescence detection of Cr(VI) [14]. A Zr-MOF-based electrochemical sensor for the detection of Cr(VI) was reported [15]. Among them, electrochemical method with the advantages of fast response rate and high sensitivity exhibits great practical application potential.

Coordination polymers (CPs) are a class of crystalline materials consisting of metal ions (or metal clusters) and organic ligands, which have been widely used for gas adsorption and separation [16], luminescence [17], magnetism

Xiaohui Li and Bingqian Wang are equally contributed to this work.

✉ Guocheng Liu
lgch1004@sina.com

✉ Xiuli Wang
wangxiuli@bhu.edu.cn

[1] College of Chemistry and Materials Engineering, Professional Technology Innovation Center of Liaoning Province for Conversion Materials of Solar Cell, Bohai University, Jinzhou 121013, People's Republic of China

[2] Key Laboratory of Cluster Science Ministry of Education, Beijing Key Laboratory of Photoelectronic/Electrophotonic, Advanced Research Institute of Multidisciplinary Science, School of Chemistry and Chemical Engineering, Beijing Institute of Technology, Beijing 100081, People's Republic of China

[18], electrochemical sensing [19] and catalysis [20], etc. Especially, CPs are promising electrocatalytic sensors because of their unique features such as adjustable structure, stable framework, abundant active sites, and easy functionalization [21]. Several Co-CPs have been reported for the electrochemical sensing of L-cysteine with low detection limits [22]. And highly selective electrochemical sensing of Ni-CP for dopamine has been discovered [23]. Cu-CPs have been used to detect H_2O_2, glucose and 2,4-dichlorophenol by the electrochemical method [24–26]. Therefore, it is highly expectant to achieve the rapidly electrochemical sensing of AA and Cr(VI) by regulating the composition and structure of CPs.

In this work, different metals (Co, Ni and Cu) were selected to construct electrochemically active CPs by coordinating with N,N′-bis(pyridine-3-ylmethyl)-4-(4-carboxybenzyl)oxybenzamide (L) and 5-nitroisophthalic acid (5-NIPA). Three 2D complexes [Co(L)(5-NIPA)(H_2O)]·H_2O (**1**), [Ni(L)(5-NIPA)(H_2O)]·H_2O (**2**) and [Cu(L)(5-NIPA)]·H_2O (**3**) were obtained by the hydrothermal method. Subsequently, CPs **1**–**3** were prepared as carbon paste electrodes to detect AA and Cr(VI), and highly sensitive and selective sensing performances were observed.

Experimental section

Synthesis of coordination polymers (CPs 1–3)

Preparation of [Co(L)(5-NIPA)(H_2O)]·H_2O (1)

A mixture of $CoCl_2·6H_2O$ (0.0475 g, 0.2 mmol), L (0.045 g, 0.1 mmol), 5-NIPA (0.021 g, 0.1 mmol), NaOH (1.5 mL, 0.1 M), and H_2O (5.5 mL) was added into a 25-mL Teflon-lined reaction kettle and heated at 100 °C for 4 days. After cooling to room temperature, massive purple crystals of **1** (22% yield based on Co) were achieved. Calculated value of $C_{35}H_{31}CoN_5O_{11}$: C, 55.56; H, 4.13; N, 9.26%. Found: C, 55.38; H, 3.97; N, 9.09%. IR (KBr, cm^{-1}): 3368 m, 2917w, 1644 s, 1525 s, 1500 s, 1436 m, 1335 s, 1295 m, 1172 m, 1108 w, 1036 w, 917 w, 844w, 726 w.

Preparation of [Ni(L)(5-NIPA)(H_2O)]·H_2O (2)

$NiCl_2·6H_2O$ (0.048 g, 0.2 mmol), L (0.045 g, 0.1 mmol), 5-NIPA (0.021 g,0.1 mmol), NaOH (3.2 mL, 0.1 M), and H_2O (6.8 mL) were added into a 25-mL Teflon-lined reaction kettle and reacted for 3 days at 150 °C. When cooled to room temperature, green lump crystals of **2** were produced with a yield of 24% (based on Ni). Calculated value of $C_{35}H_{31}NiN_5O_{11}$: C, 55.58; H, 4.13; N, 9.26%. Found: C, 55.41; H, 3.95; N, 9.01%. IR (KBr, cm^{-1}): 3376 m, 2917w,1644 s, 1516 s, 1495 s, 1351 s, 1270 m, 1223 m, 1172 m, 1104 m, 1036 m, 844 w, 729 m.

Preparation of [Cu(L)(5-NIPA)]·H_2O (3)

$CuCl_2·2H_2O$ (0.0340 g, 0.2 mmol), L (0.045 g, 0.1 mmol), 5-NIPA (0.021 g, 0.1 mmol), NaOH (3.6 mL, 0.1 M), and H_2O (6.4 mL) were added into a 25-mL Teflon-lined reaction kettle and heated in an oven at 120 °C for 4 days. After allowing to cool to room temperature, massive blue crystals of **3** were obtained with a yield of 23% (based on Cu). Calculated value of $C_{35}H_{29}CuN_5O_{10}$: C, 56.56; H, 3.93; N, 9.42%. Found: C, 55.39; H, 3.76; N, 9.23%. IR (KBr, cm^{-1}): 3368 m, 2938w, 1636 s, 1530 s, 1500 s, 1432 m, 1347 s, 1232 m, 1176 m, 1113 w, 921 w, 836 w, 785 w, 726 w, 696 w.

Preparation of carbon-paste electrodes of 1–3 (1–3CPEs)

A mixture of 15 mg of the title complex and 100 mg of graphite powder was placed in an agate mortar and ground thoroughly for about 1 h. Paraffin wax (about 1 mL) was then added and mixed well to obtain a paste-like mixture. The paste mixture was then placed in a glass tubem, and electrical contact was established by a polished copper rod. Finally, the shiny electrode surface was polished with weighing paper.

Results and discussion

Description of structural features for CPs 1–3

The single-crystal X-ray diffraction analysis shows that CPs **1** and **2** have the same space groups ($P2_1/n$), crystal systems (monoclinic), coordination environments, topology structures and similar crystallographic parameters (Table 1). In **1** and **2**, each metallic ion [M=Co(II) for **1** and Ni(II) for **2**] is six-coordinated by three carboxylic O atoms, one coordination water and two N atoms from the pyridyls of L to form typical octahedral coordination patterns (Fig. 1a and b). The Co−O distances are in the range of 2.040(2) Å–2.421(2) Å. The corresponding Ni−O distances are in the range of 2.0510(17) Å–2.2856(19) Å. The Co−N and Ni−N distances are from 2.066(2) Å to 2.111(2) Å (Tables S1–S2). The bond length of the Ni-related coordination bonds in CP **2** is slightly shorter than that of Co(II) in CP **1**, mainly because the atomic radius of

Table 1 Crystallographic data for complexes **1**–**3**

Complexes	**1**	**2**	**3**
Empirical formula	$C_{35}H_{31}CoN_5O_{11}$	$C_{35}H_{31}NiN_5O_{11}$	$C_{35}H_{29}CuN_5O_{10}$
F_w	756.58	756.35	743.17
CCDC	2,167,798	2,167,807	2,167,801
Crystal system	monoclinic	monoclinic	triclinic
Space group	$P2_1/n$	$P2_1/n$	P^{-1}
a(Å)	17.9988(12)	17.8787(7)	11.5706(11)
b(Å)	10.0281(7)	10.0681(4)	12.2156(12)
c(Å)	18.0928(12)	18.1057(7)	12.7384(11)
α(°)	90	90	108.698(2)
β(°)	95.0410(10)	95.4050(10)	100.457(2)
γ(°)	90	90	95.580(2)
V(Å^3)	3253.0(4)	3244.6(2)	1653.6(3)
Z	4	4	2
$_{Dcalc}$(g/cm^3)	1.545	1.544	1.493
μ/mm^{-1}	0.601	0.671	0.729
F(000)	1564.0	1560.0	766.0
R_{int}	0.0490	0.0354	0.0346
R_1[a] [I > =2σ (I)]	0.0431	0.0395	0.0625
wR_2[b] (all data)	0.1133	0.1369	0.1815
GOF	1.020	0.935	1.018
Δ ρ_{max}(e·Å^{-3})	0.349	0.573	0.828
Δ ρ_{min}(e·Å^{-3})	− 0.335	− 0.338	− 0.687

[a]$R_1 = \Sigma||F_o| - |F_c||/\Sigma|F_o|$. [b]$wR_2 = \Sigma[w\,(F_o^2 - F_c^2)^2]/\Sigma[w\,(F_o^2)^2]^{1/2}$

Ni(II) is slightly smaller than that of Co(II). When Cu(II) with a smaller ionic radius is selected to combine with L and 5-NIPA, CP **3** with two crystallographically independent Cu(II) ions is obtained. In CP **3**, Cu1 is six-coordinated by four carboxylic O atoms and two N atoms from the pyridyls of L to form typical octahedral coordination pattern (Fig. 1a and b). Cu2 is four-coordinated by two carboxylic O atoms and two N atoms from the pyridyls of L to form quadrilateral coordination pattern (Fig. 1a and b). The Cu−O distances are in the range of 1.908(3) Å to 2.489(3) Å. The Cu−N distances are 1.988(4) Å and 2.026(4) Å (Tables S3). In **1** and **2**, the N atoms are in the *cis*-position of the octahedral coordination conformation, and the bond angles of N−M−N are 94.15(10)° and 93.47(9)°, respectively, while the N atoms in **3** are in the *trans*-position with the N−M−N bond angles of 180°. In CPs **1**−**3**, metal ions are all extended into 1D metal-carboxylate chains through 5-NIPA, but 5-NIPA anions are on the same side of the metal-carboxylate chains in **1**−**2**, and on both sides of the chain in **3** (Fig. 1c). Owing to the conformational flexibility of the ether group (−O−) and three methylene groups (−CH_2−) in L, the metal ions are both extended into 1D helical chains through L in **1**−**2**, but one wave like Cu-L chain was obtained in **3**. (Fig. 1d and e). Finally, the metal-carboxylate chains and metal-L chains are extended into regular (for **1**−**2**) and twisted (for **3**) (4,4)-connected networks by co-metallic centers. The above in-depth structural analysis shows that the metal ions have obvious guiding effect on the structures of the title complexes.

Characterization of CPs 1–3

The infrared (IR) spectra of CPs **1**–**3** are shown in Fig. S1. The characteristic peaks appearing at 3376, 3368, 3368 cm^{-1} for the CPs **1**–**3** are assigned to the stretching vibrations of the N–H bond from the amide group in L ligand [27]. The characteristic peaks of C–N bond in pyridine ring of L ligand are present at 1636–1644 cm^{-1} [28]. The stretching vibration of nitro appears at 1530–1500 cm^{-1} [29]. The absorption peaks at 1200–1300 cm^{-1} are attributed to the antisymmetric stretching vibration of the ether bond in L ligand, and the peaks of symmetric stretching vibration appear at 1036, 1045, 1045 cm^{-1} [30]. The characteristic peaks of –CH_2– in L ligand locate at 2917, 2917 and 2938 cm^{-1}, respectively [31].

The powder X-ray diffraction (PXRD) patterns of **1**–**3** were measured to determine the purity of CPs **1**–**3** and the crystallinity of bulk crystals. As shown in Fig. S2, the diffraction peaks of as-prepared **1**–**3** are basically consistent with the simulated ones, indicating the great phase purity and crystallinity of CPs **1**–**3**. The differences in peak intensity may be due to the change of preferred orientation of crystals [32].

The thermal stability of CPs **1**–**3** was characterized by the thermogravimetric analysis (TGA). As shown in Fig. S3, the weight loss before 170 °C is attributed to the loss of the crystallization and coordination water in CPs **1**–**3**. The thermal stability can reach to about 300 °C for CP **1**, 310 °C for CP **2** and 250 °C for CP **3**, respectively, after which the frameworks of CPs **1**–**3** collapse.

Cyclic voltammograms of 1–3CPEs

Cyclic voltammetry (CV) curves of CPs **1**–**3** modified carbon paste electrodes (**1**–**3**CPEs) were measured at different scan rates (20–500 mVs^{-1}) in the electrolyte solution of 0.1 M H_2SO_4 + 0.5 M Na_2SO_4 aqueous solution. As shown in Fig. 2 and S4, a pair of reversible redox peaks exists in

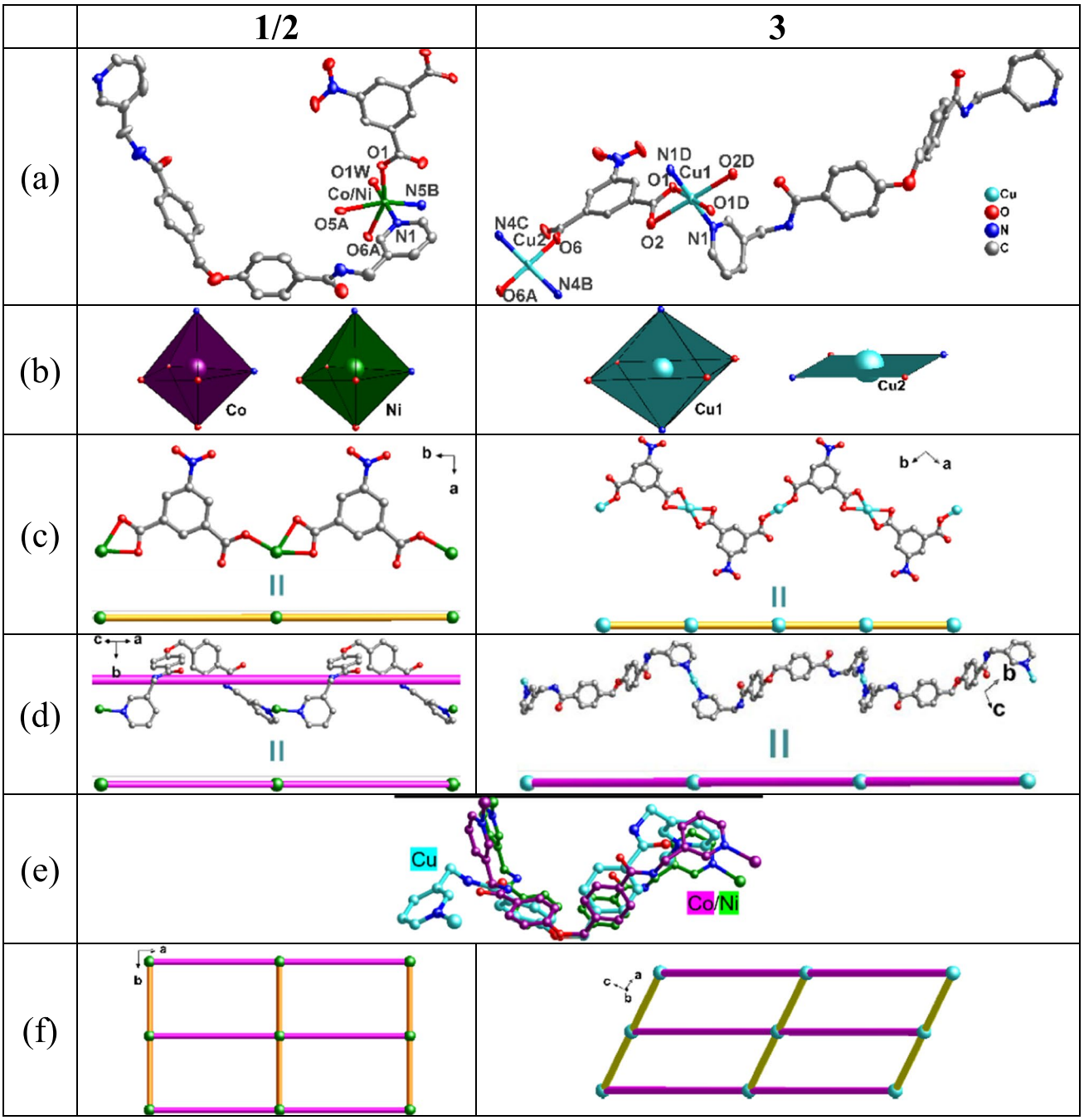

Fig. 1 The crystal structures of CPs **1**–**3**. **a** and **b** The coordination environments of metal ions [M = Co(II), Ni(II) and Cu(II)] in CPs **1**–**3**. **c** M-(5-NIPA) units. **d** M-L units. **e** Polytorsional features of amides in **1**–**3**. **f** The topology structures

CV curves of all three carbon paste electrodes in the point range from 600 to − 200 mV. The average peak potentials $E_{1/2} = (E_{pa} + E_{pc})/2$ of **1**–**3**CPEs are 271, 240 and 250 mV, respectively, belonging to the redox processes of Co, Ni and Cu centers in CPs **1**–**3** [33–35]. In addition, the peak currents of **1**–**3**CPEs increase as the scan rate increases and are approximately linearly correlated with the scan rate, proving that the redox process of CPs **1**–**3** is surface controlled [36].

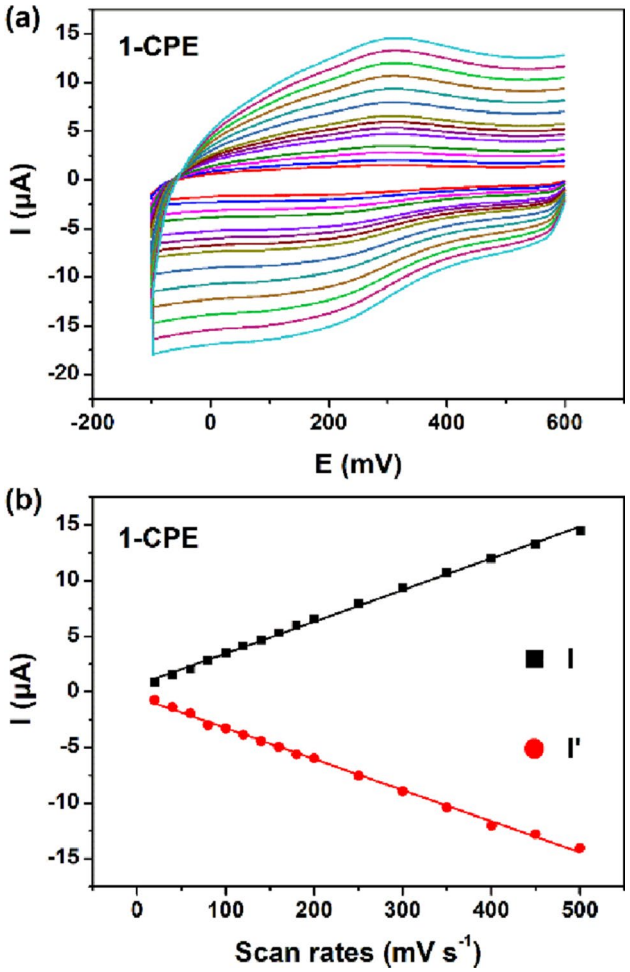

Fig. 2 **a** CV curves of **1**-CPE in the electrolyte solution of 0.1 M H_2SO_4 + 0.5 M Na_2SO_4 aqueous solution at different scan rates (20–500 mV s^{-1}). **b** Linearity of current versus scan rates for **1**-CPE

Catalytic properties for AA

The electrocatalytic properties of the three complexes for AA were investigated owing to fast and convenient detection of electrochemical method. As shown in Fig. 3a, S5a and S6a, the oxidation peak current of **1**–**3**CPEs gradually increased with the increase in AA concentration, and the corresponding reduction peak current gradually decreased. Compared to the **1**–**3**CPEs, bare electrode composed of Cu-wire with carbon past (bare-CPE) presented low electrocatalytic activity for AA sensing (Fig. S7), manifesting the great electrocatalytic oxidation behavior of CPs **1**–**3** toward AA. In addition, the current responses of **1**–**3**CPEs with continuous addition of different concentrations of AA solution with 30-s interval were monitored at optimal voltages (Fig. 3b, S5b and S6b). It was found that the response current exhibited an excellent linear relationship with the concentration of AA (5–1000 μM) in Fig. 3c, S5c and S6c. According to the equation (S/N = 3), the detection limits (LOD) of **1**–**3**CPEs for AA were 0.320, 3.360 and 3.600 μM, respectively (Table S4). The differences of **1**–**3**CPEs in electrochemical sensing capabilities may be due to the differences of morphology, roughness and defect sites on the surfaces of the modified electrodes, and different composition and structure of complexes [37–39].

The selectivity of electrochemical sensors in the real environment is an important indicator to evaluate their performances. Some of potentially interfering substances including glucose, sodium citrate, sodium thiosulfate and fructose were added to the electrochemical sensing system of AA (Fig. 3d, S5d and S6d). The results showed that the response of current was weak in all cases when these interfering substances were added. Thus, it can be demonstrated that **1**–**3**CPEs possess excellent selectivity for the electrochemical detection of AA.

Catalytic properties for Cr(VI)

The electrocatalytic performances of **1**–**3**CPEs for Cr(VI) were also explored. The reduction peak currents of **1**–**3**CPEs gradually enhanced and the corresponding oxidation peak currents weakened with the increase in Cr(VI) concentration (Fig. 4a, S8a and S9a). At the same condition, the low electrocatalytic sensing performance of bare-CPE for Cr(VI) was observed (Fig. S10), indicating the excellent electrocatalytic reduction activity of CPs **1**–**3** for Cr(VI). As shown in Fig. 4b, S8b and S9b, **1**–**3**CPEs exhibited satisfactory current responses with continuous addition of different concentrations of Cr(VI) at optimal voltages with 30-s interval. The great linear relationship between current and Cr(VI) concentration (5–150 μM) was observed in all of **1**–**3**CPEs (Fig. 4c, S8c and S9c). The detection limits of **1**–**3**CPEs for Cr(VI) concentration were calculated (0.2349, 0.9928 and 3.6054 μM, respectively), which presented the same order as that of AA (**1** < **2** < **3**) and low LOD values compared to reported working electrodes (Table S4). Furthermore, the selective sensing of **1**–**3**CPEs for Cr(VI) *vs* interfering substances (Na^+, Cd^{2+}, Co^{2+}, Ca^{2+} and Cu^{2+}) was investigated. The unchanged current response for these interfering substances demonstrated the excellent electrochemical detection selectivity of **1**–**3**CPEs for Cr(VI) (Fig. 4d, S8d and S9d).

The stability of CPs **1–3** was demonstrated by the PXRD patterns of recycled electrode materials. As shown in Fig. S11, the X-ray diffraction peaks of recycled CPs

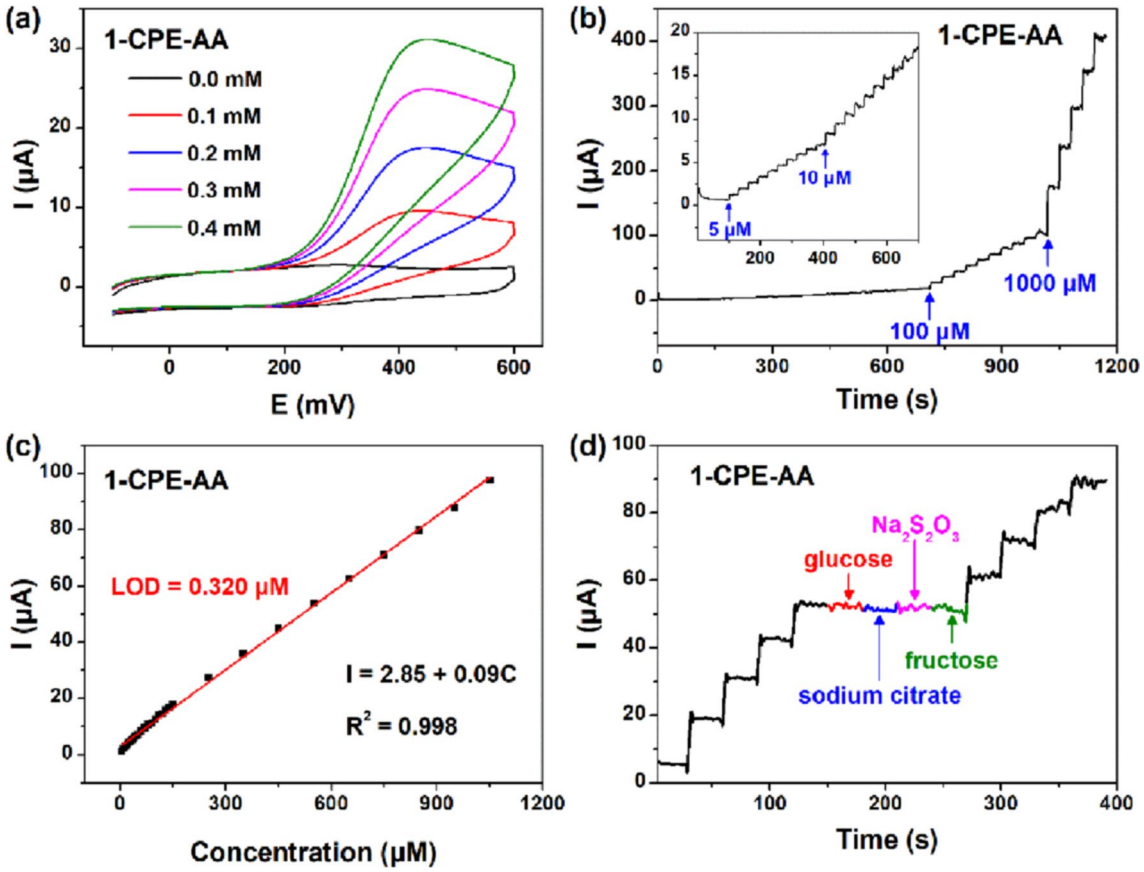

Fig. 3 **a** CV curves of **1**-CPE in 0.1 M H_2SO_4 + 0.5 M Na_2SO_4 electrolyte solution including different concentrations of AA (scan rate of 60 mV s^{-1}). **b** Current response of **1**-CPE with continuous addition of different concentrations of AA solution. **c** Calibration curve between current and concentration of AA measured by **1**-CPE. **d** Current response of **1**-CPE to AA and potentially interfering substances

1–3 were consistent with the simulated ones and the low peak intensity was due to the low content of CPs **1–3** in electrode materials. These results indicated the outstanding stability of CPs **1–3** in the electrochemical sensing process of AA and Cr(VI).

Conclusion

In summary, three 2D complexes were prepared by selecting different metal centers (Co, Ni and Cu) assembling with amide ligand L and dicarboxylic acid co-ligand 5-NIPA. These complexes exhibited outstanding electrochemical sensing properties for AA and Cr(VI) with the detection limits of 0.320, 3.360 and 3.600 μM for AA and 0.2349, 0.9928 and 3.6054 μM for Cr(VI), respectively. The design and synthesis of these complexes provide new candidates for highly efficient and selective detection of AA in human body and Cr(VI) in environment.

Supporting materials

Supporting materials includematerials, characterization, X ray crystallography, andadditional tables and figures for the s tructures and performances of CPs **1**–**3** . CCDC2167798, 2167807 and 2167801 contains the supplementary crystallographic data forCPs **1**–**3**. These data can be obtained free of charge viahttp://www.ccdc.cam.ac.uk/conts/retrieving.html, or from the CambridgeCrys tallographic Data Centre, 12 Union Road, Cambridge CB2 1EZ, UK; fax: (+44)1223 336 033; or e mail: deposit@ccdc.cam.ac.uk.

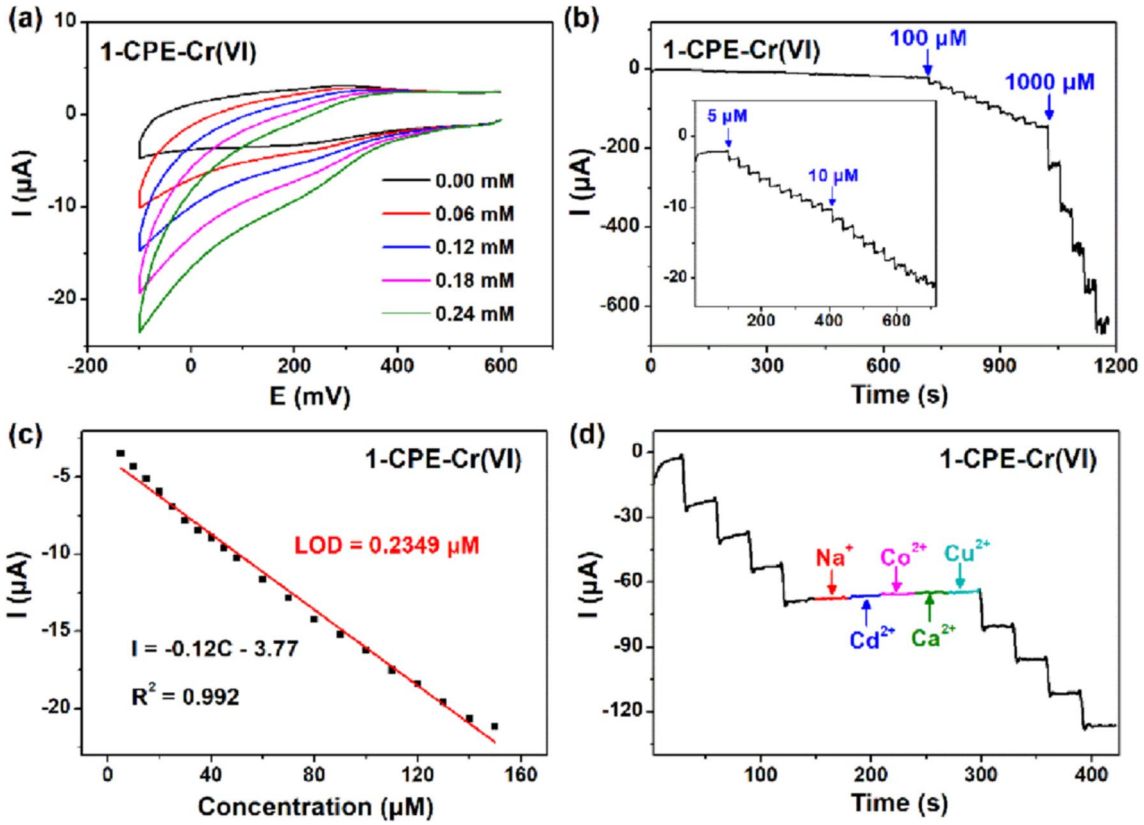

Fig. 4 **a** CV curves of **1**-CPE in 0.1 M H_2SO_4 + 0.5 M Na_2SO_4 electrolyte solution including different concentrations of Cr(VI) (scan rate of 60 mV s^{-1}). **b** Current response of **1**-CPE with continuous addition of different concentrations of Cr(VI) solution. **c** Calibration curve between current and concentration of Cr(VI) measured by **1**-CPE. **d** Current response of **1**-CPE to Cr(VI) and potentially interfering substances

Supplementary Information The online version contains supplementary material available at https://doi.org/10.1007/s11243-023-00544-9.

Acknowledgements This work was financially supported by the National Natural Science Foundation of China (21401010, 21971024, 22271021, 22201021), Education Department and the Natural Science Foundations of Liaoning province (LJ2020008, 2021-MS-312) and the Doctoral Scientific Research Foundation of Liaoning Province (2022-BS-302).

Authors' contributions XL and BW are contributed equally to this work. XL and BW prepared the main part of the manuscript, YG drew the pictures of Figures 1–4 and the supporting parts, and GL drew all the tables. X-L Wang revised the first draft of the manuscript. All authors reviewed the manuscript.

Data availability Not applicable.

Declarations

Conflict of interest The authors declare no competing financial interest.

Ethical approval Not applicable.

References

1. Meister A (1992) On the antioxidant effects of ascorbic acid and glutathione. Biochem Pharmacol 44:1905–1915
2. Chen Q, Espey MG, Sun AY, Pooput C, Kirk KL, Krishna MC, Khosh DB, Drisko J, Levine M (2008) Pharmacologic doses of ascorbate act as a prooxidant and decrease growth of aggressive tumor xenografts in mice. Proc Natl Acad Sci 105:11105–11109
3. Guo X, Yue G, Huang J, Liu C, Zeng Q, Wang L (2018) Label-free simultaneous analysis of Fe(III) and ascorbic acid using fluorescence switching of ultrathin graphitic carbon nitride nanosheets. ACS Appl Mater Interfaces 10:26118–26127
4. Dayan AD, Paine AJ (2001) Mechanisms of chromium toxicity, carcinogenicity and allergenicity: review of the literature from 1985 to 2000. Hum Exp Toxicol 20:439–451
5. Pavesi T, Moreira JC (2020) Mechanisms and individuality in chromium toxicity in humans. J Appl Toxicol 40:1183–1197
6. Li Y, Javed R, Li R, Zhang Y, Lang Z, Zhao H, Liu X, Cao H, Ye D (2023) A colorimetric smartphone-based sensor for on-site AA detection in tropical fruits using Fe-P/NC single-atom nanoenzyme. Food Chem 406:135017
7. Salem MAS, Khan AM, Manea YK, Qashqoosh MTA, Alahdal FAM (2023) Highly efficient iodine capture and ultrafast fluorescent detection of heavy metals using PANI/LDH@CNT nanocomposite. J Hazard Mater 447:130732
8. Gökmen V, Kahraman N, Demir N, Acar J (2000) Enzymatically validated liquid chromatographic method for the determination

of ascorbic and dehydroascorbic acids in fruit and vegetables. J Chromatogr A 881:309–316
9. Ferreira LMR, Cunha-Oliveira T, Sobral MC, Abreu PL, Alpoim MC, Urbano AM (2019) Impact of carcinogenic chromium on the cellular response to proteotoxic stress. Int J Mol Sci 20:4901
10. Bodylska W, Fandzloch M, Szukiewicz R, Lukowiak A (2022) Cation-exchange in metal-organic framework as a strategy to obtain new material for ascorbic acid detection. Nanomaterials (Basel) 12:4480
11. Guo L, Liu Y, Kong R, Chen G, Liu Z, Qu F, Xia L, Tan W (2019) A Metal-organic framework as selectivity regulator for Fe^{3+} and ascorbic acid detection. Anal Chem 91:12453–12460
12. Yue D, Zhao D, Zhang J, Zhang L, Jiang K, Zhang X, Cui Y, Yang Y, Chen B, Qian G (2017) A luminescent cerium metal-organic framework for the turn-on sensing of ascorbic acid. Chem Commun 53:11221–11224
13. Menon S, Usha SP, Manoharan H, Kishore PVN, Sai VVR (2023) Metal-organic framework-based fiber optic sensor for chromium(VI) detection. ACS Sens 8:684–693
14. Li Z-J, Ju Y, Wu X-L, Li X, Qiu J, Li Y, Zhang Z-H, He M-Y, Zhang L, Wang J-Q, Lin J (2023) Topological control of metal–organic frameworks toward highly sensitive and selective detection of chromate and dichromate. Inorg Chem Front 10:1721–1730
15. Ranjith Kumar D, Karthik R, Dhakal G, Nguyen VQ, Lee J, Shim J-J (2022) Catechol redox couple functionalized metal-organic framework UiO-66-NH_2 as an efficient catalyst for chromium ion sensor in water samples. J Clean Prod 374:133731
16. Lee HJ, Cho W, Jung S, Oh M (2009) Morphology-selective formation and morphology-dependent gas-adsorption properties of coordination polymer particles. Adv Mater 21:674–677
17. Liu GC, Li Y, Chi J, Xu N, Wang XL, Lin HY, Chen YQ (2020) Multi-functional fluorescent responses of cobalt complexes derived from functionalized amide-bridged ligand. Dyes Pigm 174:108064
18. Ohtani R, Yoneda K, Furukawa S, Horike N, Kitagawa S, Gaspar AB, Muñoz MC, Real JA, Ohba M (2011) Precise control and consecutive modulation of spin transition temperature using chemical migration in porous coordination polymers. J Am Chem Soc 133:8600–8605
19. Kempahanumakkagari S, Vellingiri K, Deep A, Kwon EE, Bolan N, Kim K-H (2018) Metal–organic framework composites as electrocatalysts for electrochemical sensing applications. Coord Chem Rev 357:105–129
20. Yang L, Zhang Z, Zhang C, Li S, Liu G, Wang X (2022) An excellent multifunctional photocatalyst with a polyoxometalate–viologen framework for CEES oxidation, Cr(vi) reduction and dye decolorization under different light regimes. Inorg Chem Front 9:4824–4833
21. Karmakar A, Hazra S, Pombeiro AJL (2022) Urea and thiourea based coordination polymers and metal-organic frameworks: synthesis, structure and applications. Coord Chem Rev 453:214314
22. Wu H, Shen Q, Dong J, Zhang G, Sun F, Li R (2022) Anion-regulated cobalt coordination polymer: construction, electrocatalytic hydrogen evolution and L-cysteine electrochemical sensing. Electrochim Acta 420:140442
23. Yan T, Zhang X-Y, Zhao Y, Sun W-Y (2023) Stable Zr(iv) coordination polymers with electroactive metal-terpyridine units for enhanced electrochemical sensing dopamine. J Mater Chem A 11:268–275
24. Zhang D, Zhang J, Zhang R, Shi H, Guo Y, Guo X, Li S, Yuan B (2015) 3D porous metal-organic framework as an efficient electrocatalyst for nonenzymatic sensing application. Talanta 144:1176–1181
25. Zhou B, Liang L-M, Yao J (2015) Nanoflakes of an aminoacid-based chiral coordination polymer: synthesis, optical and electrochemical properties, and application in electrochemical sensing of H_2O_2. J Solid State Chem 223:152–155
26. Dong S, Suo G, Li N, Chen Z, Peng L, Fu Y, Yang Q, Huang T (2016) A simple strategy to fabricate high sensitive 2,4-dichlorophenol electrochemical sensor based on metal organic framework $Cu_3(BTC)_2$. Sens Actuators, B Chem 222:972–979
27. Ehrhard AA, Gunkel L, Jäger S, Sell AC, Nagata Y, Hunger J (2022) Elucidating conformation and hydrogen-bonding motifs of reactive thiourea intermediates. ACS Catal 12:12689–12700
28. Yang L, Wang F, Auphedeous DY, Feng C (2019) Achiral isomers controlled circularly polarized luminescence in supramolecular hydrogels. Nanoscale 11:14210–14215
29. Yang Y, Tu C, Liu Z, Wang J, Yang X, Cheng F (2021) 5-Nitroisophthalic acid based Co(II)-coordination polymers: structural diversity tuned by imidazolyl ligands, efficient dye degradation and luminescence sensing. Polyhedron 206:115339
30. Wang J-M, Zhang P-F, Cheng J-G, Wang Y, Ma L-L, Yang G-P, Wang Y-Y (2021) Luminescence tuning and sensing properties of stable 2D lanthanide metal–organic frameworks built with symmetrical flexible tricarboxylic acid ligands containing ether oxygen bonds. CrystEngComm 23:411–418
31. Gu X, Xue D (2006) Selected controlled synthesis of three-dimensional 4d–f heterometallic coordination frameworks by lanthanide carboxylate subunits and silver centers. Cryst Growth Des 6:2551–2557
32. Okada K, Mori K, Fukatsu A, Takahashi M (2021) Oriented growth of semiconducting TCNQ@$Cu_3(BTC)_2$ MOF on $Cu(OH)_2$: crystallographic orientation and pattern formation toward semiconducting thin-film devices. J Mater Chem A 9:19613–19618
33. Patra AK, Mukherjee R (1999) Bivalent, trivalent, and tetravalent nickel complexes with a common tridentate deprotonated pyridine bis-amide ligand. Molecular structures of nickel(II) and nickel(IV) and redox activity. Inorg Chem 38:1388–1393
34. Pandey S, Das PP, Singh AK, Mukherjee R (2011) Cobalt(II), nickel(II) and copper(II) complexes of a hexadentate pyridine amide ligand. Effect of donor atom (ether vs. thioether) on coordination geometry, spin-state of cobalt and M(III)-M(II) redox potential. Dalton Trans 40:10758–10768
35. Salimi A, Alizadeh V, Hadadzadeh H (2004) Renewable surface sol-gel derived carbon ceramic electrode modified with copper complex and its application as an amperometric sensor for bromate detection. Electroanalysis 16:1984–1991
36. Antonio MR, Chiang M-H (2008) Stabilization of plutonium(III) in the preyssler polyoxometalate. Inorg Chem 47:8278–8285
37. Gaikar PS, Navale ST, Jadhav VV, Shinde PV, Dubal DP, Arjunwadkar PR, Stadler FJ, Naushad M, Ghfar AA, Mane RS (2017) A simple wet-chemical synthesis, reaction mechanism, and charge storage application of cobalt oxide electrodes of different morphologies. Electrochim Acta 253:151–162
38. McCord CP, Summers B, Henry CS (2021) Redox behavior and surface morphology of polystyrene thermoplastic electrodes. Electrochim Acta 393:139069
39. Li C, Shen J, Wu K, Yang N (2022) Metal centers and organic ligands determine electrochemistry of metal-organic frameworks. Small 18:2106607